IRANIAN JOURNAL OF PHYSICS RESEARCH

Iranian Journal of Physics Research, Vol. 6, No. 3, 2006

The puzzling Hg family revisited: a comprehensive study based on density functional theory

C Ambrosch-Draxl[1] and E Ya Sherman[2]

1. Chair of Atomistic Modelling and Design of Materials, University of Leoben, Erzherzog-Johann-Strasse 3, A-8700 Leoben, Austria
E-mail: cad@mu-leoben.at
2. Department of Physics, University of Toronto, 60 St. George Street, Toronto, Ontario, Canada M5S 1A7

(Received 2 July 2006; accepted 1 September 2006)

Abstract

We review theoretical investigations of high-temperature superconductors which have been performed by density functional theory. The main subject of our study is the Hg-based family of the superconducting cuprates, which demonstrates unusual and still puzzling properties. We show that the first-principles approach is able to describe the effects of chemical doping and pressure on the structural properties, the band structure, the ion charges, and the chemical bonds. We report on the origin of the optimal doping and present results on the inhomegeneity of the charge distribution and the concomitant splitting of the electronic bands and their contributions to the density of states. Due to their individual energy dependence, the role of the intrinsic inhomogeneities for superconductivity strongly depends on the energy and character of the quasiparticle mediating the Cooper pairing. The evolution of the electric field gradients with doping is analyzed and compared to nuclear resonance experiments. The calculated results can explain the origin of doping-induced effects observed either by local or macroscopic experimental probes. From a systematic study of the density of states by varying the doping concentration as well as applying pressure up to 15 GPa, and comparison with the measured critical temperatures, the coupling constant of the quasiparticle has been estimated to be of the order of one. Moreover, we show how density functional theory allows for the calculation of vibrational properties and phonon Raman scattering in the high-T_c cuprates. All results are quantitatively compared to experiment, and have revealed very good agreement.

Keywords: density functional theory, Hg-based high-T_c cuprates, superconductivity, pressure, doping, inhomogeneities

1. Introduction

Twenty years and thousands of publications after the discovery of high temperature superconductivity, we are far from fully understanding this class of materials. Their industrial application has been realized, but only to a very small extent compared to the initial forecast. Their ground state and superconducting properties are still not well enough known, and, in particular, the mechanism leading to the Cooper pairing is still a mystery, even though a considerable number of models have been proposed. Nevertheless, many experimental and theoretical investigations have solved a variety of puzzling questions. Among them, computational studies based on density functional theory (DFT) could contribute to the present understanding of these materials. Going back to the very beginning of the high T_c era, neither the computers nor the computer codes have been efficient enough to allow for the investigation of complex problems. It actually took a year on the fastest computers to run a self-consistent calculation for $YBa_2Cu_3O_7$th a reasonable precision. Nevertheless, early calculations helped to understand the basic features of the band structures and Fermi surfaces of several cuprates, which have been summarized and discussed in detail by Pickett in 1989[1]. At the same time, the underestimation of correlation effects by the local density approximation led to doubts about the applicability of DFT for these materials. In particular, the antiferromagnetic and insulating behaviour of their undoped parent phases could not be reproduced by LDA calculations. Only a few years later, it was shown that not only the electron density [2-4], but also optical spectra [5,6], phonons [7-12], and Raman spectra [13-15] could be obtained in a reliable way. Most of these studies were done for the fully doped $YBa_2Cu_3O_7$ or for the simplest representative La_2CuO_4. Also strain [16], as well as pressure effects [17] were investigated for the former.

Doping is the most crucial parameter to determine the critical temperature in high T_c cuprates. The metallic state is reached by doping of the parent dielectric through the replacement of ions or by introducing excess oxygen. The dopant adds states at the Fermi level E_F. As a result, E_F is shifted down thereby changing the carrier

concentration in the CuO_2 planes. The same carriers participate in the superconducting pairing. A universal relationship between T_c/T_c^{max} and the hole content among the *p*-type high T_c superconductors, was presented in Ref. [18]. This dependence is characterized by a plateau, where the variation of T_c/T_c^{max} is independent of the compound considered. Similar correlations between the doping and band structure related parameters like p_s/m^* and T_c, with p_s and m^* being the carrier density and the effective mass, respectively, are generic features of high T_c cuprates and other families of superconductors [19].

In 1993, a new family of cuprates has been discovered. The transition temperatures of the mercury-based compounds, $HgBa_2Ca_{n-1}Cu_nO_{2n+2}$, are the highest observed [20,21]. They are, however, not only fascinating for still holding the world record for T_c, which is above 160 K, but also for the fact that this quantity strongly depends on parameters like doping, the number of CuO_2 layers *n*, and pressure [22]. Hence this homologous series is ideally suited for systematically studying all these effects as well as their interplay. Although the mercury based high T_c compounds are not explicitly included in the experimental analysis described above [18,19] one can expect them to fit into this very general framework. Therefore, the mercury based compounds are used in this article to review some recent and complex DFT studies on high T_c cuprates. Thereby, we focus on structural data, the band structure and density of states (DOS), as well as the charge distribution as a function of composition, doping, and pressure. We investigate the creation of holes in the CuO_2 planes and analyze their connection to the superconducting transition temperature. Moreover, phonons and electron-phonon coupling studied within DFT are discussed.

2. Computational methods

All calculations were performed within the full-potential linearized augmented plane-wave (FP-LAPW) method as implemented in the WIEN2k code [23]. Exchange and correlation effects are accounted for by the local density approximation (LDA) parameterized by Perdew and Wang [24]. For the computational details like number of basis functions, convergence criteria, k-mesh, etc. we refer to the different papers on the doping and pressure dependence [25-27].

The LAPW method divides space into two regions: Spheres, which are centered around the atomic position S_α, and the interstitial region in between. Within the sphere α, the wave function is expanded into products of radial functions and spherical harmonics:

$$\phi_{\mathrm{k+G}}(\mathbf{S_\alpha}+\mathbf{r}) = \sum_{lm} [A_{lm}^{\alpha}(\mathbf{k}+\mathbf{G}) u_l^{\alpha}(\boldsymbol{r}, E_l) + B_{lm}^{\alpha}(\mathbf{k}+\mathbf{G}) \dot{u}_l^{\alpha}(r, E_l)] Y_{lm}(\hat{\mathbf{r}}). \quad (1)$$

Here, the functions $u_l^{\alpha}(r, E_l)$ are the solutions of the radial Schrödinger equation for the spherical part of the potential, and $\dot{u}_l^{\alpha}(r, E_l)$ are their energy derivatives

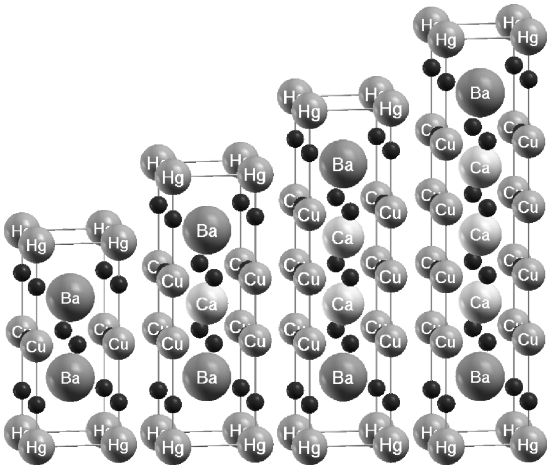

Figure 1. Unit cells of the compounds Hg-1201, Hg-1212, Hg-1223, and Hg-1234 (from left to right). Black little spheres correspond to oxygen atoms.

taken at the same energy parameter E_l [28,29]. The coefficients $A_{lm}^{\alpha}(\mathbf{k}+\mathbf{G})$ and $B_{lm}^{\alpha}(\mathbf{k}+\mathbf{G})$ are determined for each atom by matching the two basis functions in value and slope to a plane-wave $e^{i(\mathbf{k}+\mathbf{G})\mathbf{r}}$ at the sphere boundary.

This expansion allows to analyze the charge inside the spheres not only according to their atomic origin, but also with respect to their angular momentum decomposition in *l* and *m*. Charges can then be split up into e.g. p_x, p_y, p_z, $d_{x^2-y^2}$, d_{z^2}, d_{xy} ,…. Note that these partial charges depend on the chosen sphere sizes. However, they can still be used to study trends, when the sphere size is kept constant. This is important for pressure studies, where the unit cell volume decreases. It complicates the interpretation of the partial charges, since the amount of charge (volume) lying within the spheres with respect to the total charge (volume) becomes larger.

3. Crystal structures

The Hg-family is depicted in figure 1, where the layered structure becomes clearly visible. The main building block of all these compounds are the CuO_2 planes, which are responsible for the superconducting properties. All structures crystallize in a tetragonal lattice with space group *P*4/*mmm*, where the *c* axis is perpendicular to the CuO_2 planes. A short notation for the different representatives is given according to the number *n* of CuO_2 layers as Hg-12(*n*-1)*n*, i.e. Hg-1201, Hg-1212, Hg-1223, and Hg-1234 for the four members shown in figure 1. Thereby, "1" stands for one Hg and "2" for two Ba atoms in each cell. The (*n*-1) Ca atoms, and the *n* CuO_2 planes further determine this nomenclature. Throughout the manuscript, the CuO_2 layers are counted ascending from bottom to top. Atoms in the first layer are therefore referred to as Cu^1 and O^1 (even in the one-layer material) and in the second layer as Cu^2 and O^2. The apical oxygen

Table 1. Experimental data for the Hg-1201, Hg-1212, Hg1223, and Hg-1234 systems under ambient pressure. Given are the lattice constants a and c, the unit cell volume V, and the reference to the corresponding experiment.

Compound	Ref.	a [a.u.]	c [a.u.]	V [a.u.^{3}]	c/a
Hg-1201	[30]	7.332	18.000	967.7	2.455
Hg-1212	[31]	7.300	23.995	1278.7	3.287
Hg-1223	[32]	7.278	29.790	1578.0	4.093
Hg-1234	[33]	7.278	35.890	1901.1	4.931

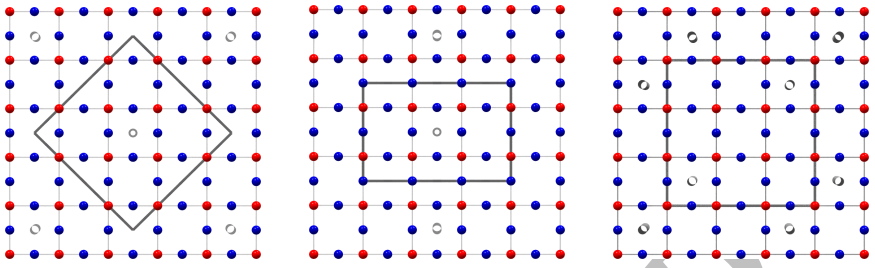

Figure 2. (color online) Copper-oxygen planes of the $HgBa_2CuO_{4+\delta}$ supercells representing the doping concentrations of δ=0.125, 0.167, and 0.22, respectively. The unit cells are indicated by the bold grey lines, the copper (oxygen) atoms by the grey (dark grey) spheres. The projection of the dopant oxygen (located at the Hg plane) onto these planes is marked by the grey circles.

will be denoted O^a in the text, while O^d will refer to the dopant oxygen. Experimental values for the lattice constants a and c can be found in Table 1.

The Hg-1201 compound has 5 inequivalent atoms in its unit cell and 8 in total. Inserting one Ca atom and one CuO_2 layer leads to Hg-1212 with its 6 inequivalent atoms (12 atoms in total). Higher compounds are generated by adding further units of Ca atoms and CuO_2 planes. Upon adding more layers, a is very similar for all systems, but with a tendency to decrease.

In order to study doping effects, supercells of the 8-, 6-, 9-, and 4-fold size compared to the undoped case have been considered [27]. By this, the inhomogeneity of the charge distribution could be studied in detail. The CuO_2 planes of the corresponding supercells for doping concentrations of $\delta = 0.125$, 0.167, and 0.22 are given in figure 2. They are chosen such that the separation of dopants is maximal, and thus minimizes the Coulomb energy of their interaction. The particular environment with respect to the dopant makes the various copper and oxygen sites within the CuO_2 planes inequivalent. The coordinates of these different types of Cu and O atoms will be provided in Section 5 (Table 3) for the structures shown in figure 2. Due to the short-ranged character of the carriers in the high-T_c cuprates, the interaction of the dopant with its surrounding is screened at an in-plane length scale which is approximately the distance between the dopant and the CuO_2 plane [33]. Hence this interaction is short-ranged. Therefore the sizes of the chosen supercells have been demonstrated to be big enough to study the effects of charge redistribution caused by the dopant ions.

The importance of structural properties for the superconducting mechanism has been pointed out in Ref. [34] in detail. It was claimed that, in order to delocalize carriers in the partially filled conduction band, the Cu-O distance should be between 3.54 and 3.72 a.u. under ambient pressure. Therefore, the response of the lattice to doping and pressure is of great interest and is now discussed from a theoretical point of view.

Oxygen doping has been considered only for the one-layer compound. The complexity of the supercells shown above hampered the full relaxation of the crystal structure. For this purpose, the virtual crystal approximation has been used, where the geometry for doping levels of δ=0, 0.08, 0.17, and 0.23 was optimized [25] by relaxing the c/a ratios and the internal coordinates with the doping dependent unit cell volumes [35] as a starting point. With respect to pressure, the structural parameters a and c have been investigated for the material containing up to four CuO_2 planes. The lattice parameters have been obtained through total energy calculations by varying them around the experimental values given in Table 1. For each configuration, the internal parameters, i.e. atomic forces, were relaxed. The resulting energy surface was then fitted to third order polynomials in a and c to determine the lattice parameters for each hydrostatic pressure point.

The results are summarized in Table 2. Due to the different procedures in relaxing the structural properties, the δ=0 and the P=0 data are not the same for Hg-1201.

The main doping effect on the crystal structure is a displacement of Ba and the apical oxygen in z-direction. This redistribution of bond lengths could be explained within an ionic picture: With increasing oxygen content, the positive Ba ions are more attracted by the oxygen, whereas the negatively charged O^a ions are further repelled. The shift of the Ba layer towards the basal plane, the shrinkage of the unit cell, a shortening of the lattice parameter a, an increase of c for small doping levels followed by a nearly linear decrease, as well as a reduction of the distance between the layers of Ba and O^a are the main trends, which are all in agreement with experimental observations [35,36].

Table 2. Calculated structural data for Hg-1201 as a function of doping, [25] and for Hg-1201, Hg-1212, Hg1223, and Hg-1234 as a function of pressure [26]. The values marked by an asterik are experimental data (see text).

Compound	δ	a [a.u.]	c [a.u.]	V [a.u.^{3}]	c/a	z_{Ba} [c]	$z_{\mathrm{O^a}}$ [c]
Hg-1201	0.00	7.2894	18.3734	976.3*	2.533	0.3003	0.2014
	0.08	7.2171	18.5554	966.5*	2.571	0.2965	0.2023
	0.17	7.1919	18.3090	947.0*	2.546	0.2851	0.2055
	0.23	7.2399	18.0665	947.0*	2.410	0.2808	0.2074
	P[GPa]						
Hg-1201	0	7.2071	17.7212	920.5	2.459		
	5	7.0844	17.0555	856.0	2.408		
	10	6.9769	16.4123	798.9	2.352		
	15	6.8804	15.7825	747.1	2.294		
Hg-1212	0	7.1674	23.6301	1213.9	3.297		
	5	7.0706	22.8189	1140.8	3.227		
	10	6.9844	22.0346	1074.9	3.155		
	15	6.9060	21.2684	1014.4	3.080		
Hg-1223	0	7.1654	29.5065	1515.0	4.118		
	5	7.0877	28.5878	1436.1	4.033		
	10	7.0178	27.6940	1363.9	3.946		
	15	6.9539	26.8186	1296.9	3.857		
Hg-1234	0	7.0888	35.2930	1773.5	4.979		
	5	6.9824	34.1299	1664.0	4.888		
	10	6.8866	33.0170	1565.8	4.794		
	15	6.7987	31.9367	1476.2	4.697		

Table 3. Copper and oxygen types, their multiplicities M, their (X,Y) coordinates given in lattice constants A and B of the respective supercells, and their in-plane distances to the nearest dopant oxygen $d_{\mathrm{O^d}}$, where a is the single cell lattice parameter. h_s denotes the number of holes created by doping at the given site, $V_{\gamma\gamma}$ are the diagonal components of the electric field gradient tensor in 10^{21} V/m^2 units, and η is the corresponding asymmetry parameter. The principal axes of the EFG are either identical or close to the crystal axes.

δ	ion	M	X	Y	d_{O}	h_s [e]	V_{11}	V_{22}	V_{33}	η
0.125	Cu^{1-1}	4	$\frac{1}{4}$	0	$a\sqrt{10}/2$	0.0515	2.6	2.6	-5.2	0.01
	Cu^{1-2}	4	$\frac{1}{4}$	$\frac{1}{2}$	$a\sqrt{2}/2$	0.0636	3.2	3.2	-6.4	0.00
	O^{1-1}	4	$\frac{1}{8}$	$\frac{1}{8}$	$3a/2$	0.0038	14.2	-8.8	-5.4	0.24
	O^{1-2}	8	$\frac{1}{8}$	$\frac{3}{8}$	$a\sqrt{5}/2$	0.0089	14.5	-8.8	-5.7	0.22
	O^{1-3}	4	$\frac{3}{8}$	$\frac{3}{8}$	$a/2$	0.0139	15.0	-8.9	-6.1	0.19
0.167	Cu^{1-1}	2	0	$\frac{1}{4}$	$a\sqrt{10}/2$	0.0591	3.0	2.8	-5.8	0.02
	Cu^{1-2}	4	$\frac{1}{3}$	$\frac{1}{4}$	$a\sqrt{2}/2$	0.0730	3.5	3.5	-7.0	0.01
	O^{1-1}	4	$\frac{1}{6}$	$\frac{1}{4}$	$a\sqrt{5}/2$	0.0087	14.7	-9.0	-5.7	0.22
	O^{1-2}	2	$\frac{1}{2}$	$\frac{1}{4}$	$a/2$	0.0195	15.5	-9.1	-6.4	0.18
	O^{1-3}	1	0	$\frac{1}{2}$	$3a/2$	0.0079	14.6	-9.0	-5.6	0.23
	O^{1-4}	2	$\frac{1}{3}$	$\frac{1}{2}$	$a/2$	0.0165	15.3	-9.1	-6.2	0.19
	O^{1-5}	1	0	0	$a\sqrt{13}/2$	0.0084	14.7	-9.0	-5.7	0.23
	O^{1-6}	2	$\frac{1}{3}$	0	$a\sqrt{5}/2$	0.0121	14.9	-8.9	-6.0	0.20
0.22	Cu^{1-1}	1	0	0	$a\sqrt{2}/2$	0.0863	3.6	3.9	-7.5	0.04
	Cu^{1-2}	4	$\frac{1}{3}$	0	$a\sqrt{2}/2$	0.0853	4.0	3.8	-7.8	0.02
	Cu^{1-3}	2	$\frac{1}{3}$	$\frac{1}{3}$	$a\sqrt{2}/2$	0.0775	3.6	3.6	-7.2	0.01
	Cu^{1-4}	2	$\frac{2}{3}$	$\frac{1}{3}$	$a\sqrt{10}/2$	0.0757	3.4	3.4	-6.8	0.00
	O^{1-1}	4	$\frac{1}{6}$	0	$a/2$	0.0253	15.7	-9.2	-6.6	0.16
	O^{1-2}	2	$\frac{1}{2}$	0	$a\sqrt{5}/2$	0.0166	15.0	-9.0	-6.0	0.19
	O^{1-3}	4	$\frac{1}{3}$	$\frac{1}{6}$	$a/2$	0.0241	15.6	-9.2	-6.4	0.17
	O^{1-4}	4	$\frac{2}{3}$	$\frac{1}{6}$	$a\sqrt{5}/2$	0.0164	15.1	-9.1	-6.0	0.21
	O^{1-4}	4	$\frac{1}{2}$	$\frac{1}{3}$	$a\sqrt{5}/2$	0.0151	15.0	-9.1	-5.9	0.21

The calculated lattice constants under ambient pressure are somewhat smaller than the experimental ones (Table 1), thus showing the typical overbinding effect of the LDA. More important, however, is that the c/a ratios are given reliably. This is the case for the other systems as well, i.e. Hg-1212, Hg-1223, and Hg-1234, although the experiments get more complicated as the number of CuO_2 layers and problems like impurities and deficiencies [31,37] increase. In case of Hg-1201, the change of volume with respect to pressure is almost linear up to 10 GPa, which had been observed before by Novikov and co-workers [38].

For all compounds the change in the lattice parameters under pressure is quite anisotropic. In general, going from ambient pressure to 15 GPa, a shrinks by about 4% while c decreases by about twice as much, i.e. the layers absorb most of the pressure by shrinking the inter-layer distance. This is in good agreement with experimentally found compressibilities [32,39,40]. Further analysis revealed that nearly the whole change in the c parameter is due to the change of the Cu-O^a bond, while the Hg-O^a bond is rather rigid upon applying pressure. For the n=2, 3, and 4 layer material the situation is similar, where in agreement with experiment [32,37] the CuO_2 planes are slightly buckled.

When relating doping to pressure, the crystalline lattice reacts in a similar way. To be more specific, the doping effect of δ=0.1 corresponds to a pressure of the order of 3 GPa. We will see below that this similarity is also reflected in the electronic structure. By increasing the number of CuO_2 planes, the in-plane lattice parameter a is decreased again. Also the insertion of a building block consisting of a CuO_2 and a Ca layer costs less space when the number of layers increases.

In addition, we mention that a comparison of the mechanical and chemical pressure and doping effects on the properties of $YBa_2Cu_3O_7$ and $YSr_2Cu_3O_7$ can be found in Ref. [41].

4. Electronic bands

The most important building block, the CuO_2 plane, provides a pd-σ band, which is intersected by the Fermi level. For the case of half-filling, this leads to a Mott-Hubbard insulator, which is however, not reproduced by DFT calculations, unless the LDA+U method is employed [42,43]. Here, we only deal with metallic cases, where the actual position of the Fermi energy inside the band depends on the doping concentration. In terms of the DOS, it is related to a local maximum of the DOS, often referred to as a van Hove singularity (vHs), which is pinned to the Fermi level in case of optimal doping. This can be seen for the fully doped compound $YBa_2Cu_3O_7$, and has been demonstrated for the Ba doped $LaCuO_4$ [44]. The same is happening in case of Hg-1201 upon oxygen doping [27,45] suggesting this to be a universal feature of the cuprates' band structure, although the charge carriers are provided in these three materials in different ways: In case of $LaCuO_4$, the three-valent La is replaced by the two-valent Ba, for $YBa_2Cu_3O_7$, the dopant is the chain oxygen, which bond to the chain copper atom has a considerable amount of covalent character, while in case of the Hg based cuprates, the doping is provided by a fully ionic [25] oxygen in the basal plane.

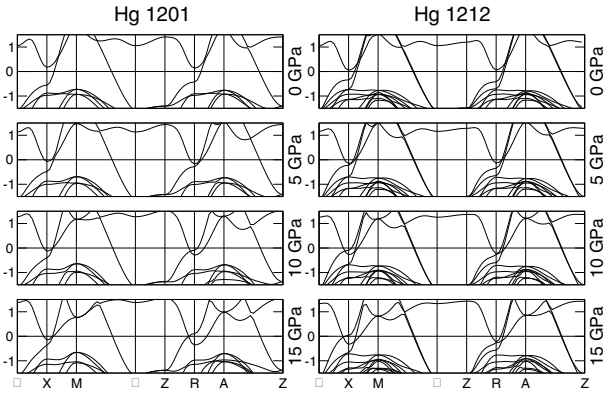

Figure 3. Band structures of Hg-1201 and Hg1212 along some high symmetry lines for pressure values up to 15 GPa.

4.1. Band structures

Among all doped single-layer cuprates, $HgBa_2CuO_{4+\delta}$ shows the highest T_c of 94 K [20]. This fact as well as the pressure dependence of T_c in this family of the superconducting cuprates, stimulated the studies of their electron band structure within DFT. Early calculations helped to understand the properties of undoped single- [46] and multi-layer [47] compounds. In addition, they demonstrated the importance of the proximity of the Fermi level to the vHs in the electron spectra of the CuO_2 planes [48], which can be achieved by applying pressure and/or by doping. The band structure and the bonding character of the dopant oxygen to the nearest Hg ion was investigated for δ=0.5 in the doped three-layer compound $HgBa_2Ca_2Cu_3O_{8+\delta}$ by supercell calculations[49].

After having already discussed the effect of doping on the electronic bands, we now turn to the pressure effect. In figure 3 the band structure of Hg-1201 is depicted along some high symmetry lines in a rather small energy window around the Fermi level, which is crossed by one CuO_2 dominated band. The band maximum can be found at M and its minimum is located at Γ. The band width is about 3.91 eV under ambient pressure and increases by almost 15% to 4.44 eV under 15 GPa. A conduction band with Hg-O^a character comes close to E_F at X and R. Upon applying pressure, it crosses the Fermi level thereby doping the $Cu^1(d_{x^2-y^2})$-O^1 (p_x) band. At the same time, the saddle point of the valence band at X and R moves up. While near the X point this saddle does not reach E_F, it crosses the Fermi level around R at about 12 GPa. A somewhat smaller value had been predicted before by Novikov [50].

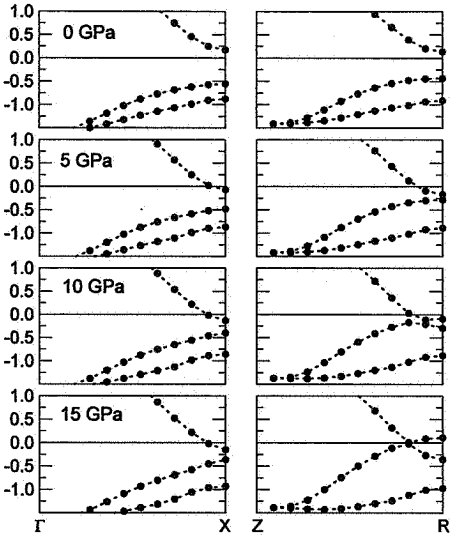

Figure 4. Band structure of Hg1201 along the high symmetry lines ΓX and ZR for different pressure values. The black filled circles mark the calculated points, where the dotted lines serve as guide to the eye. The Fermi level is set to zero and indicated by a horizontal line.

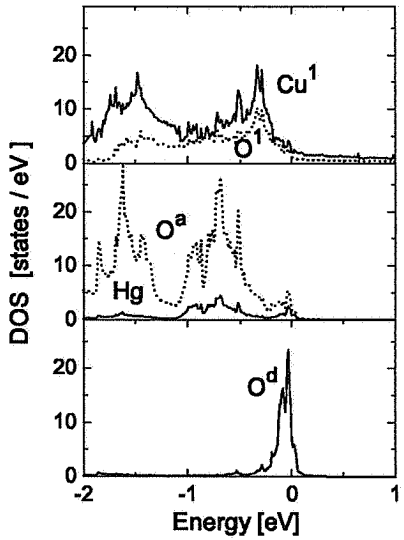

Figure 5. Site-projected densities of states in states per eV and unit cell volume V for δ=0.25 for Hg-1201 obtained by a supercell calculation containing one O^d atom per four formula units. (The Fermi level is set to zero.)

To highlight this effect, the pressure dependence of the Hg-1201 band structure around E_F along the two high symmetry lines ΓX and ZR is depicted in figure 4. Upon applying pressure, the shoulder between Z and R clearly moves up towards the Fermi level, while along ΓX the band is pushed up as well thereby getting steeper, but staying below E_F in the entire pressure range. As a result, the vHs is broadened when it arrives at E_F, which will be discussed below. Hence the vHs is pinned to the Fermi level within a certain region of the Brillouin zone (between ΓX and ZR) at high pressures which corresponds to the high and rather weakly pressure-dependent T_c in a pressure range between 10 and 20 Gpa [22,52].

For Hg1212, the band structure is also depicted in figure 3. There are now two bands corresponding to the two CuO_2 planes, which cross the Fermi level. Both bands have their maximum at M and minimum at Γ. The band widths are similar to the Hg-1201 compound, i.e. 3.92 eV under ambient pressure and 4.39 eV under 15 GPa. The Hg-O^a band almost touches E_F at ambient pressure. For this reason, all the compounds with more than one CuO_2 layers are considered to be self-doped. Similar to the one-layered compound, this effect can be increased by applying pressure. At the same time the saddle point at X moves toward E_F and crosses it at 15 GPa. Note that the points X and R are exchanged when going from the one-layered to the two-layered compound, when considering the upward movement of the bands.

For the band structures of Hg-1223 and Hg-1234, the important characteristics remain the same. Three and four CuO_2 bands, respectively, cross the Fermi level. They are hole doped through the existence of the Hg-O^a band, which shifts E_F down compared to the single-layered compound. The band extrema are similar to Hg-1201 and Hg-1212, although the increase of the band widths under pressure becomes less pronounced. Similar to the other cases, the saddle point in the valence band moves up and crosses the Fermi level. With respect to this moving at the X and R point, Hg-1223 (Hg-1234) behaves similar to Hg-1201 (Hg-1221). Details of these band structures can be found in Ref. [26].

4.1.1. Density of states

Let us turn now our attention to the DOS, which is an integral characteristic of the system and should be crucial for the transition temperature. As pointed out in Ref. [25], the increase of the hole content can be understood by ionic behavior [51] of the dopant, where the excess oxygen attracts electrons from the copper-oxygen plane thereby increasing the hole concentration in this region. The partial densities of states for δ=0.25 are shown in figure 5. It exhibits covalent bonding of Cu and the plane oxygen with peaks at -0.35 eV and a small feature right below E_F. Covalent bonds are also formed by Hg and the apical oxygen O^a, whereas the dopant atom O^d has hardly any common feature with mercury.

From the total density of states at E_F the electronic specific heat coefficient was determined. Assuming a similar behavior for other high T_c materials like the Bi-based compounds, the measured specific heat coefficient γ of $Bi_2Sr_2CaCu_2O_{8+\delta}$ as a function of doping [53] could be understood by the pronounced increase of the DOS around optimal doping. Moreover, the calculated maximum value of γ=4.4 mJ/(mol K^2) is in excellent accordance with experimental values for other high T_c materials at optimal doping [54].

Analyzing the contributions from different copper and oxygen sites it was found [27] that all of them peak at the

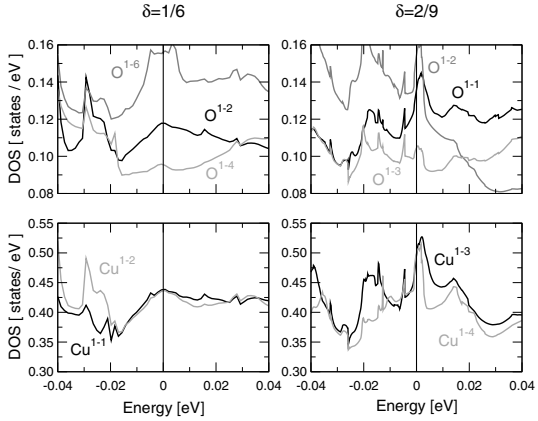

Figure 6. Selected Cu($d_{x^2-y^2}$) and O(p_x) contributions to the density of states in states per eV stemming from the respective atomic spheres for two different doping concentrations. The vertical lines indicate the Fermi level.

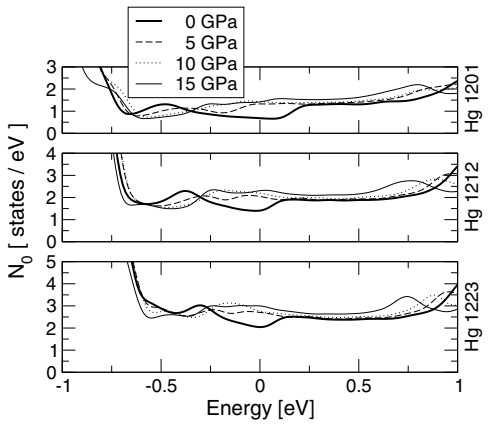

Figure 7. Density of states N in states per eV and unit cell of Hg1201, Hg1212, and Hg1223 for pressure values of 0, 5, 10 and 15 GPa.

same energy, but exhibit different behavior in the energy region around. In particular, at optimal doping, the peaks become sharper, and are sitting at the Fermi level.

To show this, the site-projected densities of states for $\delta = 0.167$ and 0.22, are presented in figure 6, highlighting the contributions of selected copper and oxygen spheres. Alike the charge carriers, the DOS's also exhibit pronounced inhomogeneities. This feature is much more pronounced when moving away from the Fermi level in the range of 0.05 eV which is a typical energy scale of quasiparticles mediating the pairing.

Similarly, the pinning of the saddle point to the Fermi level also shows up in the DOS upon applying pressure as depicted in figure 7. For Hg1201, the shoulder in the DOS is located at -0.5 eV but moving up towards E_F with pressure, where the density of states at the Fermi level N_0 is only slowly varying for higher pressure values (see figure 8). N_0 is getting larger with the number of layers, where the pressure-induced increase is nearly the same for n=1, 2, and 3. The reason for the latter fact is that with additional CuO_2 layers the corresponding bands are not fully degenerate but exhibit a certain splitting which does not allow all the corresponding shoulders to sit at E_F at the same time. Thus, the pressure-effect on the DOS is independent of the number of layers, at least up to n=3. This trend goes hand in hand with the critical temperature and with the number of holes, as we will see below.

5. Charge distribution

Without a detailed knowledge of how doping influences the number and the character of carriers, also the superconducting properties will lack a profound understanding, since the actual amount of holes is doping-determined. Yet, the knowledge about the relationship between these two physical quantities is scarce. In fact, most of the theoretical models describing high-T_c superconductivity use the hole content rather than the doping level as the input parameter. In view of being able to tune the properties of carriers and thereby T_c, a full clarification of how doping affects the electronic structure was highly desirable. In this context the questions were raised, where the excess charge goes upon doping, how doping influences the carrier concentration in the copper-oxygen planes, and what the limiting factors for the achievable amount of holes are [25].

Moreover, most theories for high T_c superconductivity make use of another simplification to describe doping effects by assuming the additional charge to be uniformly distributed within the different sites of the same atomic species in the CuO_2 plane. However, there is strong experimental evidence for intrinsic inhomogeneous charge distribution in high T_c compounds. The existence of stripes [55] in underdoped La_2CuO_4 and Bi based compounds is one clear manifestation of this inhomegeneity. In addition, there are other evidences of a spatially non-uniform charge density. Scanning tunneling microscopy experiments performed on $Bi_2Sr_2CaCu_2O_{8+\delta}$ exhibited an inhomogeneous surface carrier distribution on a length scale of 14 Å, in the normal as well as in the superconducting state, [56]. where this inhomogeneity was claimed to be an intrinsic property of this doped material, i.e. not related to impurities. More recently, it was found that the nanoscale electronic disorder in cuprates can be traced back to inhomogeneities on the atomic scale [57]. Local probes like nuclear quadrupole resonance (NQR) and nuclear magnetic resonance (NMR) experiments exhibit not only changes in the hole content with doping, but also the existence of different sites of the same species. This was seen in Tl based compounds [58] and Sr doped La_2CuO_4.[59]. Since the spatial scale of inhomogeneities is determined by the amount of dopants, for doping levels in the regime of underdoped to optimally doped, theoretical investigations on a scale of a few lattice parameters were required.

In the following, we review the results of DFT calculations on the charge distribution due to doping and pressure. Focusing on the CuO_2 planes, they have revealed, that the inhomogeneity is pronounced, occurs on

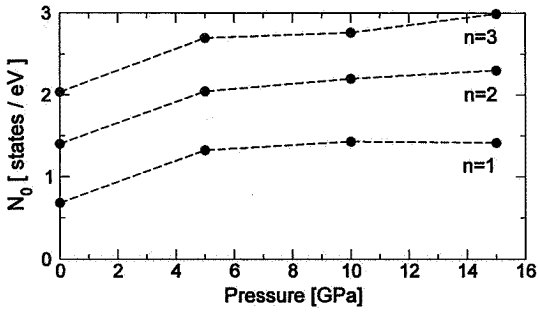

Figure 8. Density of states at the Fermi level N_0 in states per eV and unit cell in Hg1201, Hg1212, and Hg1223, for pressure values of 0, 5, 10 and 15 GPa.

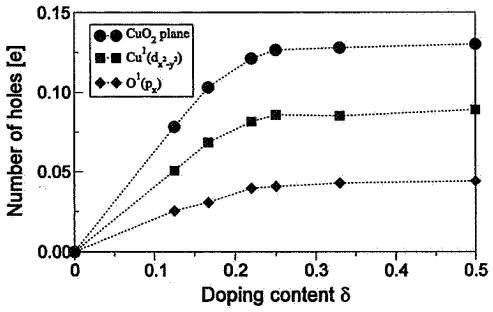

Figure 9. Doping-induced changes in the partial charges within the atomic spheres of Cu^1 and O^1, as well as the total amount of holes in the CuO_2 plane as a function of the doping concentration δ obtained by supercell calculations averaged over non-equivalent Cu and O positions.

a scale of a few lattice constants, and is strongly doping dependent. We will give an analysis of the charge distribution in the vicinity of dopant ions, where, like in the previous sections, we will start with the effects of doping followed by a pressure study and a comparison between these two parameters. Finally we will discuss how the electric field gradients are affected by doping.

5.1. Partial charges

The redistribution of the electron density upon doping is a complex process since the bonds exhibit covalent but also ionic character depending on the structural elements and atoms involved. Therefore the bonding of the crystal cannot be understood within a pure ionic model, especially since the CuO_2 planes show strong covalent character. At the same time, however, the increase of the hole content can be understood by ionic behavior [25,51] of the dopant: The excess oxygen attracts electrons from the copper-oxygen plane, thereby increasing the hole concentration in this region.

The corresponding decrease in the partial charges in the atomic spheres averaged over the respective unit cells can be seen in figure 9 and has been described in detail in Ref. [25]. It was observed that a linear increase in the total number of holes for $\delta \leq 0.22$, is followed by a plateau at higher δ values. The reason for this saturation was found in the fact that at $\delta \approx 0.22$ the dopant reaches a closed shell O^{2-} configuration. Analysis of the orbital-projected charges showed that the ratio of the additional average hole contents on $Cu(d_{x^2-y^2})$ and $O(p_x)$ orbitals h_{Cu}/h_O is approximately 4.0. With two oxygen atoms in the CuO_2 plane per chemical formula unit, it yields the amount of oxygen holes to be half that of copper.

Now we focus on the charge distribution on the atomic scale. The presence of the dopant atom makes the atomic sites chemically inequivalent, and depending on the doping level the CuO_2 $pd\sigma$ bands experience a splitting with respect to the undoped case. Accordingly, the partial charges may substantially differ from each other.

Table 3 presents the number of holes h_s created at the specific copper and oxygen sites in the CuO_2 planes with the undoped material taken as the reference. h_s strongly depends on the atomic species, the specific site, and the doping content. For all given δ values, the maximal difference in the number of doping-induced holes among non-equivalent sites of the same species (denoted as Δh_s^{max}) is approximately 0.01 e, although the distances from the ions to the next dopant may be quite different, in particular, at smaller doping concentrations. For a fixed doping content, a measure for the inhomogeneity was defined, which is Δh_s^{max} divided by the average doping-induced charge of this species (h_{Cu} or h_O, respectively). This value decreases for copper from 21% for δ=0.125 to 13% for δ=0.22, and is more pronounced for oxygen with values of 114%, 95%, and 51% for δ = 0.125, 0.167, and 0.22, respectively.

The non-uniform charge distribution can also be related to the distances to the next dopant ion. Although for all δ values the maximum amount of holes at Cu is created in the first coordination shell with the in-plane distance being $a\sqrt{2}/2$, its value strongly depends on δ. While for δ = 0.125 and 0.167 there are only two non-equivalent copper positions differing in the distance to the dopant, there are four non-equivalent Cu atoms for δ = 0.22. In this case, the biggest amount of holes is created at $Cu^{1\text{-}1}$, which is influenced by two dopant sites with the same distance. $Cu^{1\text{-}2}$ exhibits the same spacing to the nearest dopant atom, but the next nearest dopant oxygen is farther away. A similar analysis can be done for the oxygen sites. For example, at δ = 0.125, $O^{1\text{-}3}$ (at a distance of $a/2$) is most affected by the excess oxygen, followed by $O^{1\text{-}2}$, which interacts with a dopant O^d at a distance of $a\sqrt{5}/2$, and $O^{1\text{-}1}$ where the dopant is $3a/2$ away. Also for the oxygen sites the amount of created holes depends very strongly on the oxygen concentration, when positions with the same spacing to the dopant are compared. The values for the nearest dopant range from 0.0139 for δ = 0.125 to 0.0241 for δ = 0.22.

Now we turn again to the pressure effect. An increase of the $Cu^1(p_x)$ and $O^a(p_x)$ charges by 3%, indicates a strong interaction between the apical oxygen and the first

CuO_2 layer. As described earlier, this leads to the hole doping of the half filled $Cu^1(d_{x^2-y^2})$-$O^1(p_x)$ band and connects the structural properties with the band structure. Table 3 shows the corresponding partial charges for Hg-1202, Hg-1212, and Hg-1223. The copper charge in all compounds show a decrease with pressure, which, in case of the one and two-layered compound, is quite large. This effect is observed despite the fact that due to the constant atomic sphere radii a bigger fraction of the volume is inside the spheres. This suggests that the effect found is even a little underestimated. The opposite trend is found for the oxygen atoms: Increasing pressure increases the charges. This effect, however, is smaller than the decrease of the copper charges and partly originates in the constant atomic sphere radii, i.e. a bigger fraction of the volume inside the spheres under pressure.

The dependence of the charges on the number of layers *n* shows the following behavior: The Cu charges increase by inserting more layers up to three and drop again slightly by going to four layers. Note that the increase is more pronounced for higher pressures. Although the number of pressure induced holes per copper atom is smaller for the higher layered compounds, the effect is still larger there due to the higher number of layers. The oxygen charges, on the other hand, do not show a strong dependence on *n*.

Relating again pressure to doping effects, we can summarize that for both parameters, the number of holes in the CuO_2 planes is increased. While pressure mainly affects the copper orbitals, in case of doping the oxygen charges also decrease. To give a quantitative comparison for the one-layer Hg-based compound, the change in the $Cu^1(d_{x^2-y^2})$ charge of 0.05 *e* corresponds to the pressure of 15 GPa or doping $\delta \approx 0.12$. The picture for comparing pressure and composition effects is similar. By going from one to two and three layers the amount of holes per copper atom is smaller, but due to more layers, the effect is still larger for the structures with more layers. By inserting the fourth layer, the number of holes decreases again as the result of an increasing Cu^2 charge. It follows that the number of holes induced by any of the three control parameters exhibits the same behavior as the transition temperature [22].

5.2. Electric field gradients

The electron and nuclear charge densities produce a highly non-uniform electric field within the unit cell which can be probed by nuclear quadrupole and magnetic resonance. In the cuprates, this is typically at the sites occupied by ^{17}O and ^{63}Cu isotopes. A nuclear quadrupole moment *Q* is coupled to the gradients of the electric field [60] given by $V_{\alpha\beta} = \partial E_\alpha / \partial x_\beta$, where E_α is the component of the local electric field, and x_β is the Cartesian coordinate. The traceless tensor $V_{\alpha\beta}$ can be diagonalized in the principal axes as $V_{\gamma\gamma}$. The corresponding resonance at radio wave frequency (~10^8 s^{-1})

$$\omega = \frac{eQ}{2\hbar} V_{zz} (1+\eta^2/3)^{1/2}, \quad (2)$$

appears in the absorption spectrum of the system. Ordering the tensor elements by their absolute value, such that $|V_{xx}| \le |V_{yy}| \le |V_{zz}|$, the asymmetry parameter η is defined as $(V_{xx} - V_{yy})/V_{zz}$, where V_{zz} is called *the* electric field gradient EFG. The corresponding tensor components and asymmetry parameters are given in Table 3. The changes in the charge densities due to the doping affect the local electric field, and, in turn, the V_{zz} parameter. Hence the NQR lines split, and, therefore, the degree and the origin of the inhomogeneity can be traced back from the nuclear spin resonance data. Experimental data [59] on EFGs in $La_{2-x}Sr_xCuO_4$ have revealed a doping-induced upward shift of the mean copper EFG in the order of 10%, a splitting of the resonance line according to different inequivalent sites, and a decrease in the splitting of the resonant frequencies of two different Cu sites with increasing doping. One can clearly conclude from Table 3, that all these findings are consistent with the DFT results. NMR measurements on Tl-based compounds [58] exhibit changes in the copper and oxygen EFGs of the order of 10% with doping, again concomitant with the calculations. At the same time, NQR data taken on Hg1202 also revealed an upward shift with doping [61], which is, however, too large in order to be understood in terms of oxygen-doping induced holes only. It was argued that additional defects [34,62] could be responsible for such a strong increase of the resonant frequencies. The theoretical findings are also in good qualitative agreement with the experimental observations of Ref. [63] performed on under- and overdoped $HgBa_2CuO_{4+\delta}$ crystals, where a shift, a splitting, and a change of the in-plane ^{17}O NMR line width were revealed with the change of the doping concentration.

To top the picture off, we mention that the electric field gradient calculated for $La_{2-x}Ba_xCuO_4$ as a function of doping shows the largest changes, i.e. a 30% decrease in the absolute value for V_{zz} at the apical oxygen O^a site, where the η parameter for the in-plane oxygen changes from 0.38 to 0.30 by increasing *x* from zero to 0.14.

6. Lattice vibrations

Lattice vibrations in high-T_c cuprates attract attention as a factor which can influence both the normal and superconducting states, as well as possible mediators of superconductivity. Knowledge of the strength of the electron-phonon coupling and its changes with doping is crucially important for this understanding. The phonon frequencies and the matrix elements of electron-phonon coupling are determined by the effect of the ion displacements on the electron band structure. Experimentally, phonons are seen directly in the inelastic (Raman) light scattering and infrared light absorption

experiments or indirectly in the experiments probing the electron energy and decay, such as the angle-resolved photoemission spectroscopy. In the latter, however, the effects of band structure, phonon spectrum, and electron-phonon coupling are presented in the integral form, and are difficult to interpret. On the other hand, Raman scattering shows phonons with zero momentum, with well-defined frequencies, where the role of electron-phonon coupling can be clearly seen as the line broadening, lineshape, and, up to a certain extent, in the scattering intensity. Here we first shortly describe how to calculate phonon modes and electron-phonon coupling. Then we discuss the results for $YBa_2Cu_3O_7$ and the Ba doped Zurich oxide, $La_{2-x}Ba_xCuO_4$, before we again turn to the Hg based cuprates.

6.1. Phonon frequencies and eigenvectors

To find the frequencies and eigenvectors of the zero-momentum phonons, the total lattice energy $E_{\rm tot}$ can be expanded as a function of the ion displacements in the form:

$$E_{tot} = A_0 + \sum_{j,\alpha} A_j u_j^{\alpha} + \frac{1}{2}\sum_{j,\alpha}\sum_{l,\beta} A_{jl} u_j^{\alpha} u_l^{\beta} + \frac{1}{6}\sum_{j,\alpha}\sum_{l,\beta}\sum_{m,\gamma} A_{jlm} u_j^{\alpha} u_l^{\beta} u_m^{\gamma} + \ldots, \quad (3)$$

where the elements of the matrices A_j, A_{jl}, and A_{jlm} correspond to the force constants with A_{jlm} presenting the lattice nonlinearities. Here j, l, m are Cartesian indices and α, β, and γ numerate the ions. The resulting dynamical matrix can by simplified by the analysis of the irreducible representations of the unit cell symmetry group. A more efficient procedure to obtain the frequencies and eigenvectors of the Γ-point vibrations is based on the direct calculation of interatomic forces [10]. LDA calculations for the fully symmetric phonon frequencies in $YBa_2Cu_3O_7$ yielded results[7,8,10] which agree with experiment within 10-15%. An even better agreement [9] could be achieved by employing the generalized gradient corrections (GGA), and by optimizing the unit cell parameters [12]. A comparison of the LDA and the GGA results for the fully-symmetric phonons in $GdBa_2Cu_3O_7$ and $PrBa_2Cu_3O_7$ has recently been given in Ref. [41]. A very high accuracy could also be achieved for the B_{2g} and B_{3g} phonon frequencies in $YBa_2Cu_3O_7$ [15]. But not only the vibrational frequencies, but also the calculated eigenvectors turned out to be in excellent agreement with experiment [9,15].

A comprehensive analysis of the phonon frequencies as a function of Ba doping has been performed in Ref. [44]. It was found that for the high-frequency A_g and E_g modes the frequency shifts with doping less than in 1%, while for the low-frequency E_g mode associated with La/Ba vibrations the frequency is increased by a factor of two when x is close to 0.14.

The phonon modes for the Hg compounds were investigated within the PhD thesis of H. Auer [45]. According to the factor group analysis for Hg-1201, there are four Raman-active zone center modes, two of them having A_g, the other two E_g symmetry. The A_g modes for the undoped compound are nearly perfectly decoupled, such that one mode shows a pure Ba displacement, while the other one represents a vibration of the apical oxygen. Both exhibit an increase in the vibrational frequency by applying pressure: $\omega_O{}^a$ goes from 590 to 603 cm^{-1} (with one $cm^{-1} \approx 0.12$ meV), while ω_{Ba} increases from 144 to 152 cm^{-1}, when the unit cell volume is decreased by 8%, where the optimized lattice parameters have been the starting point. For Hg-1212, there are four total-symmetric modes, with vibrational frequencies of 595, 382, 147, and 81 cm^{-1}, respectively. The mode highest in frequency is an O^a vibration, the next one a nearly pure oscillation of the plane copper atom O^1, while the two lowest ones are found to be out-of-phase and an in-phase vibrations of Cu^1 and Ba, respectively. Their pressure-dependence is similar as for the Hg-1201 vibrations in the sense that all of them increase in frequency, where the effect is most pronounced for the mode lowest in energy. For Hg-1223, the five A_g modes at 592, 369, 273, 147, and 73 cm^{-1} correspond to displacements of O^a, O^1 with some out-of-phase movement of Ca, Ca with some in-phase movement of O^1, and again the out-of-phase and an in-phase vibrations of Cu^1 and Ba, respectively. For Hg-1234, 7 A_g modes are present at 599, 382, 364, 239, 142, 112, and 85 cm^{-1}. Now the second CuO_2 layer also takes part in the four vibrations lowest in energy, where the 112 cm^{-1} is clearly dominated by the Cu^2 oscillation.

Concerning the phonons, doping has only been treated by the VC approximation and for the one-layer material Hg-1201. It hardly affects the Ba mode, but dramatically decreases the apical oxygen mode in the lower doping regime, while it increases again at higher doping concentrations, i.e. in the optimal doping regime.

6.2. Raman scattering and electron-phonon coupling

Lattice vibrations can change the bandstructure of the crystal, modulate its dielectric function $\varepsilon_{jl}(\omega) = 1 + 4\pi\chi_{jl}(\omega)$ and, hence lead to the Raman scattering at the phonon frequencies. The dielectric susceptibility of the solid is determined by

$$\chi_{jl}(\omega) = \frac{2}{\hbar}\sum_{i,f}\int \langle i\mathbf{k}|M_j|f\mathbf{k}\rangle\langle f\mathbf{k}|M_l|i\mathbf{k}\rangle\left[\frac{1}{\omega_{fi}(\mathbf{k})-\omega} + \frac{1}{\omega_{fi}(\mathbf{k})+\omega}\right]\frac{d^3\mathbf{k}}{(2\pi)^3}, \quad (4)$$

where $\omega_{fi}(\mathbf{k})$ is the interband transition frequency between the initial $|i\mathbf{k}\rangle$ and final $|f\mathbf{k}\rangle$-states, $\langle i\mathbf{k}|M_j|f\mathbf{k}\rangle$ is the j component of dipole matrix element, and the summation is performed over all allowed transitions. The lattice displacements alter the dielectric susceptibility by changing the interband distances and the transition matrix elements. Therefore, the scattering intensity is a possible measure of the

electron-phonon coupling strength. Moreover, by changing the light frequency, one can see how the phonons interact with the electron states resonating with the given light frequency. LDA calculations of the phonon Raman scattering in $YBa_2Cu_3O_7$ showed a very good agreement with experiment in terms of the phonon frequencies, their scattering intensities, as well as their dependencies on the exciting photon energy [15]. The salient features of the Raman spectra of $YBa_2Cu_3O_7$ are (i) a strong Raman scattering by the vibrations of the apical oxygen ion with the frequency close to 500 cm^{-1}, when both, the incident and scattered light are polarized along the *z*-axis, (ii) similar resonant dependencies in this scattering geometry of this mode and the in-phase *z*-axis-vibrations of the plane oxygen ions at $\approx$440 cm^{-1}, and (iii) a high scattering intensity for the out-of phase vibrations along the *z*-axis of the plane oxygens at $\approx$340 cm^{-1}. All these and other findings were be reproduced and quantitatively explained by the calculation. Therefore, DFT can well describe the band structure, optical transitions, and the relevant electron-phonon coupling. The Raman intensity in $La_{2-x}Ba_xCuO_4$ showed a pronounced doping-induced increase [44]. This effect reveals the doping-related changes in the band structure and electron-phonon coupling.

An analysis of the lattice dynamics and Raman scattering in Hg-based compounds [45] based on the computational procedure introduced in Refs [9] and [15] exhibited similar trends as observed in $YBa_2Cu_3O_7$ and $La_{2-x}Ba_xCuO_4$ concerning the dependence of the Raman spectra on the band structure and agree with available experimental data [65].

Raman scattering corresponds to the electron-phonon coupling for electrons in the entire Brillouin zone and even in different electron bands. Hence the information of all electron bands within a few eV and their response to the lattice vibrations is needed. By resonant Raman scattering one can even probe the coupling of the electronic subsystem to the lattice in dependence on the energy of incoming light. The typical Raman scattering experiments are carried out with light beams in the visible region, i.e. they don't probe the energy scale of the boson, which mediates the Cooper pairing.

For the quantitative understanding of the role of electron-phonon coupling for the electron self-energy and for phonon-mediated superconductivity, the detailed information on those electronic states near the Fermi surface is required, which interact with the phonons. Therefore, the electron-phonon coupling constants should be computed for arbitrary momentum transfer within the energy scale of the boson around the Fermi level. Their estimates from first principles have been performed in early DFT calculations of the high- T_c cuprates [7,8,66,67]. Within the first-principles scheme, such calculations can be carried out within linear-response theory, where a pattern of atomic displacements is considered as a perturbation to the equilibrium configuration, and the corresponding changes in the electronic properties are obtained as a response to it. Besides simple systems, this procedure has been applied so far to the $CaCuO_2$ [68], the undoped La_2CuO_4, [11], to $YBa_2Cu_3O_7$ [69], and the most investigated superconductor of recent years, MgB_2 [70]. Its wider application to the high-T_c cuprates could be a promising tool for their understanding.

Another interesting effort [52] to obtain the coupling of the boson mediating the Cooper paring from DFT results, was made for the Hg-based family. Thereby, the knowledge of the calculated DOS was used and related to the superconducting properties of these compounds: Knowing on the one hand, the pressure dependence of N_0 from the theoretical side, and T_c from the experimental side, one could estimate the effective dimensionless coupling constant $\lambda \sim N_0$, assuming a BCS-like behavior, i.e. $T_c \sim \omega_B \exp(-1/\lambda)$, valid for the weak coupling for any type of the intermediate boson. Thereby, ω_B is the frequency of the boson. It should be noted, that the DOS does not necessarily have to be assumed to be constant near the Fermi level on the ω_B scale, but it turned out to be approximately the case and thus can be used for this estimate. There were, however, several problems which hampered a more quantitative comparison between theory and experiment. First, the pressure dependence of T_c has been measured on samples which include a doping concentration close to optimal doping, while the calculations had been performed for the undoped material. Second, there are still big uncertainties in the experimental data regarding defects and non-stoichiometry of the samples. And third, when dealing with compounds with more than one layers, it is unclear how to treat their contributions to T_c in the theoretical considerations. Despite all these uncertainties, however, conclusions were possible. From all theoretical doping studies mentioned before, i.e. for $YBa_2Cu_3O_7$, $La_{2-x}Ba_xCuO_4$[44], and $HgBa_2CuO_{4+\delta}$ [25], it was know that at optimal doping the saddle point is pinned to the Fermi level. Since in Hg-1201, the vHs reaches E_F at approximately 5GPa, this pressure value was interpreted as the effective chemical pressure corresponding to optimal doping in the sense that both, the optimal doping and this pressure lead to similar, important band structure effects in the vicinity of the Fermi level. The changes of T_c due to pressure were assumed to occur on top of the doping-induced T_c, i.e. are of the order of 10-20%. From a comparison of the pressure-induced change of T_c with the change of N_0, λ could be estimated to be of the order of one, where a possible pressure-induced enhancement of ω_B can only increase this estimated value. A electron-boson coupling constant of this order has indeed been extracted recently [71] from the analysis of electron damping observed in electron Raman spectra of $HgBa_2CuO_{4+\delta}$.

7. Summary and outlook

To summarize, we have reviewed ab-initio calculations for the electronic properties, lattice dynamics, and phonon Raman scattering in high-temperature cuprates. The method allows to directly calculate physical

observables such as densities of states, electric field gradients, optical properties, phonon modes, and Raman scattering intensities with high accuracy. All these quantities have been obtained as a function of doping and pressure, and are excellent agreement with experiment. Other important physical effects, such as the influence of doping and pressure on the superconducting properties, the origin of the optimal doping, inhomogeneity effects observed in local-probe experiments, the difference between the local and macroscopic probes, the influence of doping on the chemical bonds, the strength of electron-boson coupling, responsible for superconductivity can be either extracted from or understood on the basis of the first-principles results.

Some important recent achievements, which open new roads for first-principles calculations, have to be mentioned to give an outlook on the future abilities of these techniques. First, despite the success of all the calculations mentioned above, one should keep in mind that the treatment of strong electron correlations is still not solved. The application of LDA+U has been mentioned already in this context [72]. Also self-interaction correction has led to an improvement of the situation for the antiferromagnetic parent phases [73]. Here, dynamical mean-field theory could be an alternative route. Born as a tool to analyze the Hubbard model with the infinite number of spatial dimensions [74], it became a valuable technique for the calculation of real solids. Its success is based on the right combination of the first-principles scheme and model calculations [75-77].

Concerning superconductivity, density functional theory for superconductivity [78] is an exciting and promising tool. Density-functional theory is very general, and, therefore, it should give the correct superconducting ground state, provided the interaction between electrons is given correctly and the way to describe the macroscopically coherent superconducting state is found [79] so far, in conventional superconductors as well as MgB_2 [80], the electron-phonon coupling, as a mediator for superconductivity, has been found from these ab-initio calculations. Hence, the full treatment of the superconducting state within density functional theory has already become possible.

Acknowledgments

This work was supported by the Austrian Science Fund, projects P13430, P14004 and M591.

References

1. W E Pickett, *Rev. Mod. Phys*. **61** (1989) 433.
2. C Ambrosch-Draxl, P Blaha and K Schwarz, *J. Phys*.: *Condens. Matter*, **1** (1989) 4491-4496.
3. C Ambrosch-Draxl, P Blaha and K Schwarz, *Phys. Rev*. B **44** (1991) 5141-5147.
4. K Schwarz, C Ambrosch-Draxl and P Blaha, *Phys. Rev*. B **42** (1990) 2051.
5. J Kircher, M K Kelley, S N Rashkeev, M Alouani, D Fuchs, and M Cardona, *Phys. Rev*. B, **44** (1991) 217.
6. C Ambrosch-Draxl, R Abt and P Knoll, *Physica* C **235-240** (1994) 2119.
7. R E Cohen, W E Pickett and H Krakauer, *Phys. Rev. Lett*. **64** (1990) 2575.
8. C O Rodriguez, A I Liechtenstein, I I Mazin, O Jepsen, O K Andersen and M Methfessel, *Phys. Rev*. B **42** (1990) 2692.
9. C Ambrosch-Draxl, R Kouba and P Knoll, *Z. Phys*. B **104** (1997) 687.
10. R Kouba and C Ambrosch-Draxl, *Phys. Rev*. B **56** (1997) 14766.
11. C Z Wang, R Yu and H Krakauer, *Phys. Rev*. B **59** (1999) 9278.
12. R Kouba, C Ambrosch-Draxl and B Zangger, *Phys. Rev*. B **60** (1999) 9321.
13. E T Heyen, S N Rashkeev, I I Mazin, O K Andersen, R Liu, M Cardona and O Jepsen, *Phys. Rev*. *Lett*. **65** (1990) 3048.
14. P Knoll, C Ambrosch-Draxl, M Mayer, R Abt and E Holzinger-Schweiger, *Physica* C **235-240** (1994) 2117.
15. C Ambrosch-Draxl, H Auer, R Kouba, E Ya Sherman, P Knoll and M Mayer, *Phys. Rev*. B **65** (2002) 064501.
16. W E Pickett, *Physica* C **289** (1997) 51.
17. H Khosroabadi, M R Mohammadi Zadeh and M Akhavan, *Physica* B **321** (2002) 360.
18. H Zhang and H Sato, *Phys. Rev. Lett*. **70** (1993) 1697.
19. Y J Uemura, L P Le, G M Luke, B J Sternlieb, W D Wu, J H Brewer, T M Riseman, C L Seaman, M B Maple, M Ishikawa, D G Hinks, J D Jorgensen, G Saito and H Yamochi, *Phys. Rev. Lett*. **66** (1991) 2665.
20. S N Putilin, E V Antipov, O Chmaissem and M Marezio, *Nature* **362** (1993) 226.
21. A Schilling, M Cantoni, J D Guo and H R Ott, *Nature* **363** (1993) 56.
22. L Gao, Y Y Xue, F Chen, Q Xiong, R L Meng, D Ramirez and C W Chu, *Phys. Rev*. B **50** (1994) 4260.
23. P Blaha, K Schwarz, G K H Madsen, D Kvasnicka and J Luitz, 2001, WIEN2k, Vienna University of Technology, *An Augmented Plane Wave + Local Orbitals Program for Calculating Crystal Properties*.
24. J P Perdew and Y Wang, *Phys. Rev*. B **45** (1992) 13244.
25. C Ambrosch-Draxl, P Süle, H Auer and E Ya Sherman, *Phys. Rev*. B **67** (R) (2003) 100505.
26. T Thonhauser, H Auer, E Ya Sherman and C Ambrosch-Draxl, *Phys. Rev*. B **69** (2004) 104508.
27. C Ambrosch-Draxl and E Ya Sherman, *Phys. Rev*. B **74** (2006) 024503.
28. O K Andersen, *Phys. Rev*. B **12** (1975) 3060.
29. D D Kölling and G O Arbman, *J. Phys. F*, **5** (1975) 2041.
30. B A Hunter, J D Jorgensen, J L Wagner, P G Radaelli, D G Hinks, H Shaked, R L Hitterman and R B Von Dreele, *Physica* C **221** (1994) 1.

31. P G Radaelli, J L Wagner, B A Hunter, M A Beno, G S Knapp, J D Jorgensen and D G Hinks, *Physica* C **216** (1993) 29.
32. A R Armstrong, W I F David, I Gameson, P P Edwards J J Capponi, P Bordet and M Marezio, *Phys. Rev*. B **52** (1995) 15551.
33. T Ando, A B Fowler and F Stern, *Rev. Mod. Phys*. **54** (1982) 437.
34. E V Antipov, A M Abakumov and S N Putilin, *Supercond. Sci. Technol*. **15** (2002) 31.
35. Q Huang, J W Lynn, Q Xiong and C W Chu, *Phys. Rev*. B **52** (1995) 462.
36. A M Balagurov, D V Sheptyakov, V L Aksenov, E V Antipov, S N Putilin, P G Radaelli and M Marezio, *Phys. Rev*. B **59** (1999) 7209 and references therein.
37. R Gatt, E Olsson, A Morawski, T Lada, A Paszewin, I Bryntse, A M Grishin, Yu Eeltsev, P Berastegui and L -G Johansson, *Physica* C **276** (1997) 270.
38. D L Novikov, M I Katsnelson, Jaejun Yu, A V Postnikov, A J Freeman, *Phys. Rev*. B **54** (1996) 1313.
39. J H Eggert, J Z Hu, H K Mao, L Beauvais, R L Meng and C W Chu, *Phys. Rev*. B **49** (1994) 15299.
40. V L Aksenov, A M Balagurov, B N Wsavenko, D V Sheptyakov, V P Glazkov, V A Somenkov, S Sh Shilshtein, E V Antipov and S N Putilin, *Physica* C **275** (1997) 87.
41. H Khosroabadi, B Mossalla and M Akhavan, *Phys. Rev*. B **70** (2004) 134509.
42. P Wei and Z Q Qi, *Phys. Rev*. B **49** (1994) 12159.
43. P Blaha, K Schwarz and P Novak, *Int. J. Quant. Chem*. **101** (2005) 550.
44. T Thonhauser and C Ambrosch-Draxl, *Phys. Rev*. B **67** (2003) 134508.
45. H Auer, PhD thesis, University of Graz, (2001).
46. D L Novikov and A J Freeman, *Physica* C, **212** (1993) 233.
47. D J Singh, *Phys. Rev*. B **48** (1993) 3571.
48. D L Novikov and A J Freeman, *Physica* C, **216** (1993) 273.
49. D J Singh and W Pickett, *Phys. Rev. Lett*. **73** (1994) 476.
50. D L Novikov, O N Mryasov and A J Freeman, *Physica* C **222** (1994) 38.
51. A M Abakumov, V L Aksenov, V A Alyoshin, E V Antipov, A M Balagurov, D A Mikhailova, S N Putilin and M G Rozova, *Phys. Rev. Lett*., **80** (1998) 385.
52. C Ambrosch-Draxl, E Ya Sherman, H Auer and T Thonhauser, *Phys. Rev. Lett*. **92** (2004) 187004.
53. J L Tallon and J W Loram, *Physica* C: Superconductivity, **349** (53) 53.
54. N M Plakida, *High-Temperature Superconductivity*, Springer, Berlin (1995).
55. J M Tranquada, in *Neutron Scattering in Layered Copper-Oxide Superconductors*, edited by A Furrer (Kluwer, Dordrecht, The Netherlands, 1998) p. 225.
56. S H Pan, J P ONeal, R L Badzey, C Chamon, H Ding, J R Engelbrecht, Z Wang, H Eisaki, S Uchida, A K Gupta, K W Ng, E W Hudson, K M Lang and J C Davis, *Nature* **413** (2001) 282.
57. K McElroy, J Lee, J A Slezak, D -H Lee, H Eisaki, S Uchida and J C Davis, *Science*, **309** (2005) 1048.
58. A Gerashenko, Yu Piskunov, K Mikhalev, A Ananyev, K Okulova, S Verkhovskii, A Yakubovskii, L Shustov and A Trokiner, *Physica* C, **328** (1999) 163.
59. P M Singer, A W Hunt and T Imai, preprint *cond-mat*/0302078.
60. M H Cohen and F Reif, *Quadrupole Effects in Nuclear Magnetic Resonance Studies of Solids*, Seitz and Turnbull (Eds.), in Solid State Physics, V. 5, Academic Press, Inc., NY (1957).
61. A A Gippius, E V Antipov, W Hoffmann and K Lüders, *Physica* C **276** (1997) 57.
62. O Chmaissem, J D Jorgensen, D G Hinks, J L Wagner, B Dabrowski and J F Mitchell, *Physica* C **241-243** (1998). 805.
63. J Bobroff, H Alloul, P Mendels, V Viallet, J-F Marucco and D Colson, *Phys. Rev. Lett*. **78** (1997) 3757.
64. H Khosroabadi, A Tavana and M Akhavan, *Eur. Phys.* J. B **51** (2006) 161.
65. X Zhou, M Cardona, C W Chu, Q M Lin, S M Loureiro and M Marezio, *Phys. Rev*. B **54** (1996) 6137.
66. O K Andersen, A I Liechtenstein, O Rodriguez, I I Mazin, O Jepsen, V P Antropov, O Gunnarsson and S Gopalan *Physica* C, **185** (1991) 147.
67. H Krakauer, W E Pickett and R E Cohen, *Phys. Rev*. B **47** (1993) 1002.
68. S Y Savrasov and O K Andersen, *Phys. Rev. Lett*. **77** (1996) 4430.
69. K -P Bohnen, R Heid and M Krauss, *Europhys. Lett*. **64** (2003) 104.
70. J Kortus, I I Mazin, K D Belashchenko, V P Antropov and L L Boyer, *Phys. Rev. Lett*. **86** (2001) 4656.
71. Y Gallais, M Le Tacon, A Sacuto and D Colson, *Europhys. Lett*. **73** (2006) 594.
72. V I Anisimov, F Aryasetiawan and A I Lichtenstein, *J. Phys*.: *Condens*. Matter **9** (1997) 767.
73. Z Szotek, W M Temmerman, A Svane, L Petit and H Winter, *Phys. Rev*. B **68** (2003) 104411.
74. W Metzner and D Vollhardt, *Phys. Rev. Lett*. **62** (1989) 324.
75. V I Anisimov, A I Poteryaev, M A Korotin, A O Anokhin and G Kotliar, *J. Phys*.: *Condens. Matter*, **9** (1997) 7359.
76. A I Poteryaev, A I Lichtenstein and G Kotliar, *Phys. Rev. Lett*. **93** (2004) 086401.
77. N E Zein, S Y Savrasov and G Kotliar, *Phys. Rev. Lett*. **96** (2006) 226403.
78. N L Oliveira, E K U Gross and W Kohn, *Phys. Rev. Lett*. **60** (1998) 2430.
79. M Lüders, M A L Marques, N N Lathiotakis, A Floris, G Profeta, L Fast, A Continenza, S Massidda and E K U Gross, *Phys. Rev*. B **72** (2005) 024545, M

A L Marques, M Lüders, N N Lathiotakis, G Profeta,A Floris, L Fast, A Continenza, E K U Gross and S Massiddam, *Phys. Rev*. B (2005) 024546.

80. A Floris, G Profeta, N N Lathiotakis, M Lüders, M A L Marques, C Franchini, E K U Gross, A Continenza and S Massida, *Phys. Rev. Lett*. **94** (2005) 037004.